JOURNAL OF PROPULSION AND POWER
Vol. 16, No. 6, November–December 2000

Optimization of Orifice Geometry for Crossflow Mixing in a Cylindrical Duct

J. T. Kroll,* W. A. Sowa,† and G. S. Samuelsen‡
University of California, Irvine, Irvine, California 92697-3550
and
J. D. Holdeman§
NASA John H. Glenn Research Center at Lewis Field, Cleveland, Ohio 44135

Mixing of gaseous jets in a crossflow has significant applications in combustion science and engineering, one example of which is the mixing zone of a rich-burn/quick-mix/lean-burn gas turbine combustor. A major design question is the jet orifice shape and jet orifice number that optimizes the mixing performance. To delineate the optimal orifice features for a given axial distance and momentum-flux ratio, a statistical design of experiments test matrix was established around three variables: the number of orifices, the orifice aspect ratio, and the orifice angle (in circumferential plane). A jet-to-mainstream momentum-flux ratio of 40 and a mass-flow ratio of 2.5 were selected as representative of a practical design. To yield an interpolating equation that predicts the mixing performance of orifice geometry combinations within the range of the test matrix parameters, a regression analysis was conducted on the data. The results reveal that 1) mixture uniformity is a nonlinear function of the number of orifices, the orifice aspect ratio, and the orifice angle and that 2) optimum mixing occurs when the mean jet trajectories are in the range of $0.30 < \zeta/R < 0.5$ (where $\zeta = R - r$) at $x/R = 1$. At the optimum number of orifices, the difference between shallow-angled slots with large aspect ratios and round holes is minimal and either geometry produces optimal mixing performance.

Nomenclature

A	=	total cross-sectional area in the mixer, see Eq. (3)
AR	=	orifice aspect ratio (long to short dimension), see Fig. 2
a	=	nodal area, see Eq. (3)
C	=	constant, for example, see Eq. (1)
f	=	mixture fraction, for example, see Eq. (2)
$\bar{f}$	=	mean mixture fraction
h	=	orifice axial length
J	=	momentum-flux ratio (jet/mainstream), $(\rho_j V_j^2/\rho_\infty U_\infty^2)$
MR	=	mass-flow ratio
n	=	number of orifices
R	=	mixer radius
r	=	radial coordinate ($r = 0$ at center)
T	=	gas temperature
U_S	=	area weighted normalized variance, for example, see Eq. (3)
x	=	axial distance
α	=	orifice angle with respect to mainstream flow in $x-\theta$ plane, 0 = long axis aligned with mainstream flow
ζ	=	$R - r$ ($\zeta = 0$ at wall)
θ	=	circumferential coordinate
χ	=	regression model term, see Eq. (4)

Introduction

MIXING of air jets into a crossflow is a fundamental part of gas turbine engine technology. Combustor efficiency, exit plane temperature pattern factor, low emissions, and effluent gas composition are strongly affected by the quality of the air jet–combustor gas mixing that is achieved. One scheme for advanced, low-pollutant emission combustors is the rich-burn/quick-mix/lean-burn (RQL) method. Because a significant amount of the combustion air is injected via jets through the sidewall, optimization of the mixer must consider wall orifice distribution, orifice size, orifice shape, orifice spacing jet penetration characteristics, and local enthalpy levels due to the jet mixing characteristics. In conventional combustors, most of the important combustion mechanisms (e.g., strength and size of the recirculation zone, volumetric heat release patterns, liquid fuel evaporation and consumption characteristics) are linked to the primary jet mixing processes. Clearly, advances in gas turbine combustor technology are dependent on, and cannot occur without, improved understanding of jet mixing into confined crossflows.

The need to understand and optimize jet mixing into crossflows is not limited to gas turbine combustor applications. Similar mixing problems exist in the design of fuel and air premixers, the discharge of effluent into water, vertical/short takeoff and landing (V/STOL) aircraft in ground proximity and many other applications where two continuously flowing streams are mixed together.

The present study addresses the characteristics that govern the optimal crossflow mixing in cylindrical ducts. The goals of the present study are to 1) characterize the relationship between the jet orifice shape and number as it relates to mixture uniformity at an axial distance of one duct radius downstream of the orifice leading edge and 2) identify the optimal mixing configuration for a given momentum-flux ratio.

Background

Many studies of confined jet mixing have been conducted on combustor components for advanced gas turbine engines. Recent NASA-supported studies are summarized in works by Holdeman et al.[1,2] for cylindrical and rectangular ducts, respectively. Previous studies, mostly with smaller orifices in rectangular and annular ducts, are summarized by Holdeman.[3] A summary of previous jet-in-crossflow studies (mostly confined) is given by Margason.[4]

These summaries contain substantial reference listings, including previous works of other researchers. Therefore, only those

Received 28 April 1998; revision received 13 September 1999; accepted for publication 17 September 1999.

*Student. Member AIAA.
†Research Scientist, Department of Mechanical, Aerospace, and Environmental Engineering, Combustion Laboratory; currently Research Scientist, United Technologies Research Center. Member AIAA.
‡Professor, Director, Combustion Laboratory; gss@uci.edu. Associate Fellow AIAA.
§Senior Research Engineer. Associate Fellow AIAA.

references from which material is specifically cited are included herein. In all of these summaries the importance of the momentum-flux ratio and the spacing between adjacent orifices is delineated.

Hatch et al.[5] studied the mixing characteristics of both circular and slanted slot orifices in a cylindrical duct, where the number of orifices for each mixer was held constant at eight. Mixing quality was quantified at an axial distance equal to one duct radius downstream of the leading edge of the orifice using an area weighted standard deviation value for experimentally determined mixture fractions. The best mixer had the smallest value of area weighted standard deviation at the evaluation plane. Among other results, it was observed that the optimum mixing configuration varied in the number of orifices at a fixed momentum-flux ratio. Consequently, because the number of orifices was not varied, an optimum mixer could not be identified.

In a study limited to round hole orifices, Kroll et al.[6] determined experimentally the optimum number of orifices for momentum-flux ratios of $J = 36$ and 70. The optimum number of round hole orifices for these momentum-flux ratios based on the same criteria as the Hatch et al.[5] study was found to be 10 and 15 round hole configurations, respectively. The results agreed well with the design equation reported by Holdeman et al.[1] and Holdeman[3]:

$$n = \pi\left(\sqrt{2J}/C\right) \tag{1}$$

where $C = 2.5$ as suggested in Ref. 3.

Oechsle et al.[7] considered the optimization requirements of the different orifice designs reported by Hatch et al.[5] Oechsle et al.[7] used several different parameters for optimization including an area weighted standard deviation, and concluded that the relatively shallow-angled slanted slot orifices would provide optimum jet penetration and mixing characteristics.

Although the preceding studies have provided substantial insight on orifice optimization, none of the studies followed an optimization approach that systematically varied orifice design parameters at a fixed momentum-flux ratio such that a mathematical response surface could be created. This is the goal of the current study, namely, to identify the sensitivity of jet mixing performance to small changes in orifice slot angle, AR, and number of orifices. All orifices are rectangles with semicircular ends where, for $AR = 1$, the orifice is a round hole.

Experiment

Facility

The experimental facility that was used for this research is the same basic test stand and flow panel that is described by Hatch et al.[5,8] and Kroll et al.[6,9] This facility provided 100°C (212°F) mainstream air at atmospheric pressure. Jet air was supplied at 23°C (74°F) to a manifold that supplied the orifices in the mixer. A thermocouple probe was used to measure the local temperature where the jet fluid mixed with the heated mainstream fluid.

Figure 1 depicts the arrangement of the test assembly and the thermocouple probe. The displacement of the three axes was monitored with a Mitutoya digital displacement indicator with a precision of 0.0025 cm (0.001 in.). The 0.32-cm ($\frac{1}{8}$-in.) type K thermocouple used for thermal flowfield mapping was centered and aligned prior to each experiment.

The mainstream flow entered the bottom of the mixing module at a temperature of 100°C (212°F) and a bulk velocity of 9.4 m/s (31 ft/s). The jet air manifold was manufactured with four ports equally spaced around the manifold's circumference at both the top and bottom. Four individually metered airstreams supplied the lower four manifold ports with jet air at approximately 23°C (74°F). After entering the bottom of the manifold, the jet air flowed upward through a 1.27-cm- ($\frac{1}{2}$-in.-) thick honeycomb ring. The honeycomb aided in removing any swirl from the jet air prior to its passage through the mixer's orifices. One of the manifold's top ports was used to monitor the air pressure, a thermocouple was located in a second port to measure the jet temperature, and the remaining two ports were capped off. A dimensioned mixer is shown in Fig. 2 for reference.

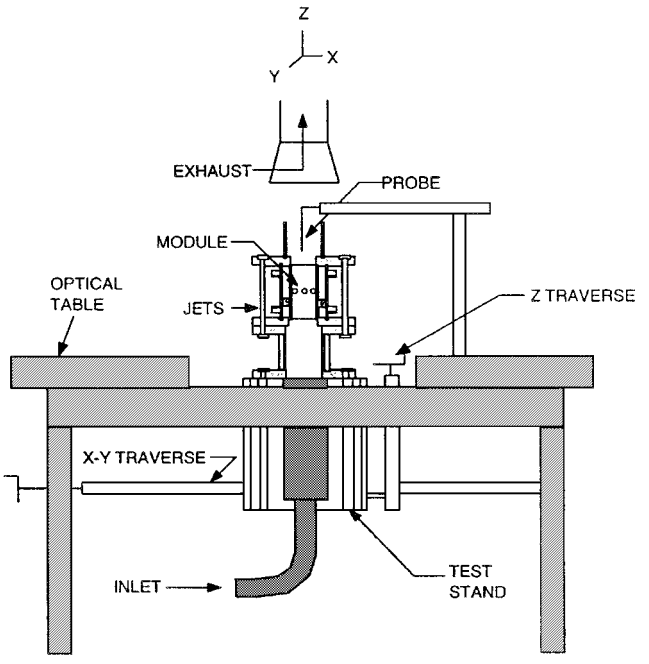

Fig. 1 Test stand schematic.

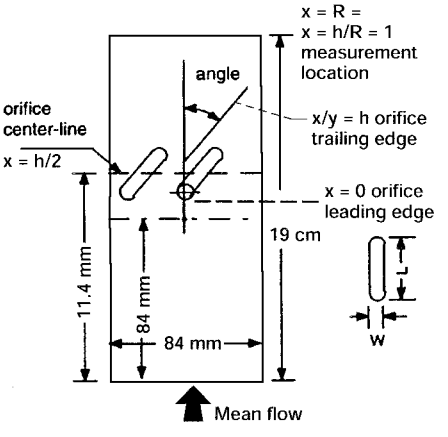

Fig. 2 Mixing module dimensions.

Measurements

A thermocouple probe was chosen to perform the point temperature measurements in accordance with the desire to use a simple and reliable measurement technique. The relatively large time constant of the thermocouple had the effect of averaging the temperature fluctuations in the fully turbulent flowfield. Four probe designs were investigated to evaluate which design minimizes flowfield perturbations. Each probe design used a 30.5-cm- (12-in.-) long, 0.32-cm- ($\frac{1}{8}$-in.-) diam type-K thermocouple. The following criteria were established to evaluate alternative probe designs:

1) The calculated jet fluid backflow should be minimized and approach zero at the orifice leading edge.

2) At the plane of the orifice trailing edge ($x/h = 1$), 100% of the jet fluid mass should be accounted for.

3) Deviation of the mean mixture fraction from the calculated equilibrium value at $x/R = 1$ should be minimized.

The initial probe design was a straight, axially aligned probe. Because this probe was aligned with the bulk fluid flow direction, it would perturb the flow the least downstream of the orifices. The experiments bore this out. For the straight, axial-aligned probe, flowfield perturbations were not significant except in the orifice region.

However, in the vicinity of the orifices, the strong degree of crossflow normal to the probe caused perturbations that resulted in the appearance of a high degree of jet fluid backflow, that is, the propagation of jet fluid in the upstream direction.

To minimize the perturbations in the orifice region, three other thermocouple probe designs were analyzed. The first was an axially aligned probe with a 90-deg bend near the thermocouple junction. In this arrangement, the 90-deg section of the probe pointed into the oncoming jet stream, thereby eliminating the strong crossflow that was problematic for the straight probe. Analysis of data collected with the 90-deg probe revealed that this arrangement was biased to the mainstream flow. Where the straight probe was unrealistically cold in the orifice region (biased to the jets), the 90-deg probe was unrealistically hot (biased to the mainstream). In both cases, the cross-stream fluid tended to bias the measurement.

The second was an axially aligned probe with a 45-deg bend. The 45-deg probe results fell almost exactly between the two extremes. Mass balance closure testing of the 45-deg probe data set revealed that 100% jet mass addition was accounted for at the orifice trailing edge. The differences between a shielded and a nonshielded thermocouple probe were also investigated. No differences were observed. Consequently, an exposed-junction, 45-deg thermocouple probe was used to acquire the entire data set reported herein.

Each of the orifice optimization experiments involved the measurement of at least six planes of data. Several planes were concentrated in the orifice region where the strongest thermal gradients were located. A limited number of only eight planes of data were acquired due to tradeoff between having enough mixing detail while keeping the time associated with each experiment to a reasonable length. The planes included $x/R = 0$, $h/2$, h, and 1 where x/R is the nondimensional downstream distance relative to the leading edge of the orifice, h/R is the orifice axial length, and R is the mixer radius. Whereas the data at all of the planes provide the perspective of jet penetration and mixing, the $x/R = 1$ plane was selected for the detailed analysis of mixture fraction. The selection of this plane 1) corresponds to prior studies, and 2) corresponds to a location in practical systems where, due to hardware constraints, mixing must be complete.

In each plane, the data were taken in a region consisting of a two-orifice sector. If the two-orifice sector was less than (greater than) 90 deg, then the grid was spatially compressed (expanded) so that the relative density of the measurements was preserved. The gridding scheme followed in this study for a 90-deg, two-orifice sector is shown in Fig. 3. The central portion of the grid is composed of a Cartesian type of scheme employing equal y and z increments. Additionally, data points are arranged in an equal increment fashion along the initial and final sector radial lines, as well as around the circumference of the sector.

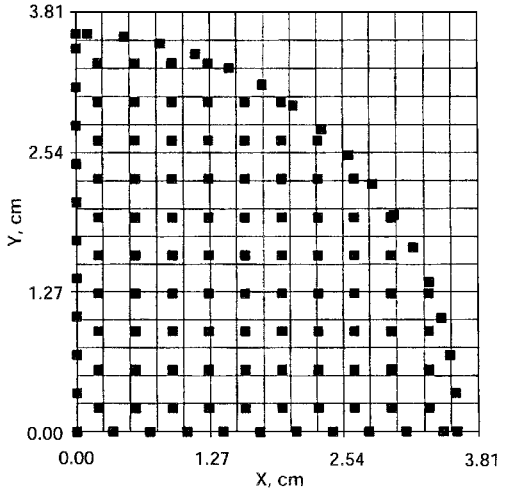

Fig. 3 Example of 90-deg, two-orifice sector planar data point grid density.

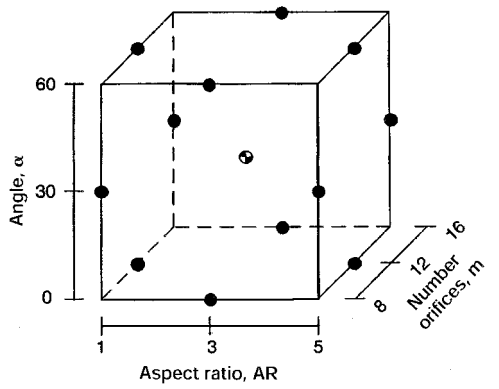

Fig. 4 Graphical illustration of Box–Behnken test matrix.

Global Orifice Optimization

On the basis of the results reported by Hatch et al.[5] and Kroll et al.,[6] a Box–Behnken test matrix was established for this study. The previous studies were used to identify parameter ranges that would encompass the optimal mixing geometry at a momentum-flux ratio of 40 and at a fixed jet-to-mainstream mass-flow ratio of 2.5. Table 1 shows the variable settings for each case considered. Three parameters were varied: number of orifices ($n = 6$, 8, 10, 12, and 16), slot aspect ratio ($AR = 1$, 3, 5), and slot angle ($\alpha = 0$, 30, 60). The first 13 experiments tabulated in Table 1 are shown in Fig. 4. The Box–Behnken test matrix allowed the fitting of nonlinear regression equations to the data while minimizing the number of required experiments. As noted, Fig. 2 details the mixer design used. In this study all of the orifices had circular ends. Consequently, a slot with an AR of 1 was corresponded to a round hole. The operating conditions are $T_{main} = 212$°F, $T_{jet} = 74$°F, $P = 14.7$ psia, $V_{main} = 31.0$ ft/s, $M_{main} = 0.090$ lbm/s, mass-flow ratio = 2.5, density ratio = 1.28, and momentum-flux ratio = 40 J.

On completion of the data acquisition for the initial 13 cases in Table 1, the unmixedness was calculated at each plane. The measurements at the $x/R = 1$ axial plane were repeated to provide an estimate of experimental error for each of the initial 13 cases. A regression analysis was performed on the results to arrive at a model that quantifies U_S as a function of the number of orifices, the orifice AR and the orifice angle. The results of this regression analysis highlighted the need to conduct a second Box–Behnken test matrix to better refine the response surface.

Cases 14–26 in Table 1 detail the second test matrix. This test matrix was identical to the first except that the number of orifices was 6, 8, and 10. This matrix was tested when analysis revealed that cases 1–13 were biased to underpenetration. Cases 14–26 were added to balance the results. When the measurements corresponding to cases 14–26 were completed, a cubic model was fit to the data sets and used to further understand the relationship between design parameters.

Analysis

The mixture fraction value is a measure of the degree of local unmixedness at a given point. Temperature measurements were made as a means of tracking the local mixture fraction. This was possible because the experiments were nonreacting. In an incompressible flow such as this, temperature is a conserved scalar; that is, no sources or sinks. Conserved scalars can track other conserved scalars (e.g., local elemental mass fractions) in a nonreacting system.[10]

The jet mixture fraction takes the following form when based on temperature:

$$f = \frac{T_{main} - T_{local}}{T_{main} - T_{jet}} \tag{2}$$

In this form, a value of $f = 0$ corresponds to the presence of pure mainstream flow, whereas $f = 1$ indicates the presence of pure jet flow. Complete mixing occurs when f approaches the equilibrium

Table 1 Box–Behnken test parameters

Case	Number of orifices, n	Orifice aspect ratio, AR	Orifice angle, α	h/R	Blockage,[a] %	Spatial unmixedness
1	16	5	30	0.639	110	0.077
2	16	3	0	0.563	47	0.065
3	16	3	60	0.375	132	0.134
4	16	1	angle-independent	0.353	90	0.110
5	12	5	0	0.826	31	0.023
6	12	5	60	0.495	144	0.126
7	12	3	30	0.592	83	0.028
8, 9	12	1	angle-independent	0.408	78	0.033
10	8	5	30	0.904	79	0.016
11	8	3	0	0.796	34	0.028
12	8	3	60	0.531	94	0.028
13	8	1	angle-independent	0.500	64	0.014
14	10	5	30	0.808	88	0.009
15	10	3	0	0.712	38	0.010
16	10	3	60	0.475	105	0.059
17	10	1	angle-independent	0.447	72	0.012
18	8	5	0	1.012	26	0.035
19	8	5	60	0.607	119	0.053
20	8	3	30	0.725	68	0.012
21, 22	8	1	angle-independent	0.500	64	0.014
23	6	5	30	1.044	68	0.039
24	6	3	0	0.919	29	0.063
25	6	3	60	0.613	82	0.013
26	6	1	angle-independent	0.577	56	0.042

[a]Blockage is defined as the sum of the circumferential projections of each orifice divided by the circumference of the mixer.

value determined by the mass-flow ratio $f_{\text{equil}} = MR/(1 + hR)$ and temperatures of the jet and mainstream.

To quantify the mixing effectiveness of each mixer configuration, a spatial unmixedness parameter U_S (Ref. 11) was defined at each measurement and interpolated data plane:

$$U_S = \frac{1/A \sum a_i (f_i - \bar{f})^2}{\bar{f}(1 - \bar{f})} \tag{3}$$

where f_i is the average planar mixture fraction, a_i is the nodal area at which f is calculated, and $A = \sum a_i$. Note that at planes downstream of the trailing edge of the orifice, $\bar{f}$ equals the equilibrium mixture fraction (0.715). Complete mixing is achieved when the U_S across a given plane reaches zero. This parameter is based on Ref. 12.

Results

In addition to configuration specifics, Table 1 lists the orifice axial length, the percentage of orifice blockage, and the spatial unmixedness for the 26 configurations considered. The dimensionless orifice axial length is expressed as the ratio of the axial projection of the orifice h to the radius of the mixing module R. The percent blockage is expressed as a ratio of the total circumferential projection of the orifices to the circumferential spacing between adjacent orifices.

The normalized orifice axial length h/R is a measure of the axial rate of jet mass addition. To illustrate its importance to mixing, consider two extreme cases, $h/R = 1$ and $h/R \approx 0$. For the case where $h/R = 1$, the jet fluid addition process is continuing right up to the mixing analysis plane at $x/R = 1$. The jet fluid that passes through the trailing portion of the orifice does not have the opportunity to mix with the main fluid. This results in warm and cool spots in the analysis plane and can cause a correspondingly high mixture fraction variance. At the other extreme is the case where $h/R = 0$. This corresponds to the jet fluid being added instantaneously, thereby having the entire residence time between $x/R = 0$ and 1 to mix with the main fluid. Note that in both the six-orifice case with $AR = 5$ and an angle of 30 deg, and the eight aligned slot case with $AR = 5$, the trailing edge of the orifice (orifice axial length) extends beyond one duct radii downstream of the leading edge. Also, in several other cases, the orifice trailing edge is at an axial distance nearly equal to one duct radius. The smallest h/R (0.353) studied experimentally was the round hole case.

The percentage of orifice blockage increases for an increasing number of orifices and an increasing slant angle when the other variables are constant. A high aspect ratio design at a 0-deg orifice inclination angle (aligned with the mixer's centerline) will have a large h/R and a small percentage of orifice blockage. The opposite is also true.

As the percentage of orifice blockage approaches 100, the jet flow approaches the point of appearing to completely inhibit the flow of the mainstream fluid near the module wall. This can have the advantage of cooling the walls at the expense of allowing an undiluted core of main fluid to pass through the mixer section, that is, underpenetration. Similarly, with an orifice angle of zero, that is, no orifice-induced swirl component, and as the percentage of orifice blockage approaches zero, the jet penetration will be greater and a large portion of the walls will be exposed to undiluted main fluid while the jets impinge on one another at the module centerline, that is, overpenetration. Slotted orifice designs at orifice angles 0 and 90 deg act as swirl vanes to the approaching main flow. In the consideration of jet penetration, the swirl component imparted on the main flow must be considered.

Mixture Fraction Contours at $x/R = 1$

The mixture fraction contour plots at an axial distance equal to one duct radius downstream of the orifice leading edge are shown in Fig. 5 for the 16-orifice case. Each case in Fig. 5 represents a two-orifice measurement sector that has been orifice averaged. Similar figures for the 12-, 10-, 8-, and 6-orifice cases are shown in Figs. 6–9, respectively. In these mixture fraction contour plots, each contour image is labeled with a numerical designator of the form: number/aspect ratio/angle. For example, 16/3/30 signifies the 16-orifice module at a AR of 3 and an orifice slant angle α of 30 deg from the mainstream flow direction. In the contour plots, a mixture fraction value of 0 corresponds to pure main flow material, a value of 1 corresponds to pure jet flow material. Because an AR of one corresponds to a round hole, the performance of an $AR = 1$ mixer is independent of orientation angle. In the figures that follow, for convenience, the $AR = 1$ cases are associated with an angle corresponding to what the Box–Behnken test matrix would call for if the

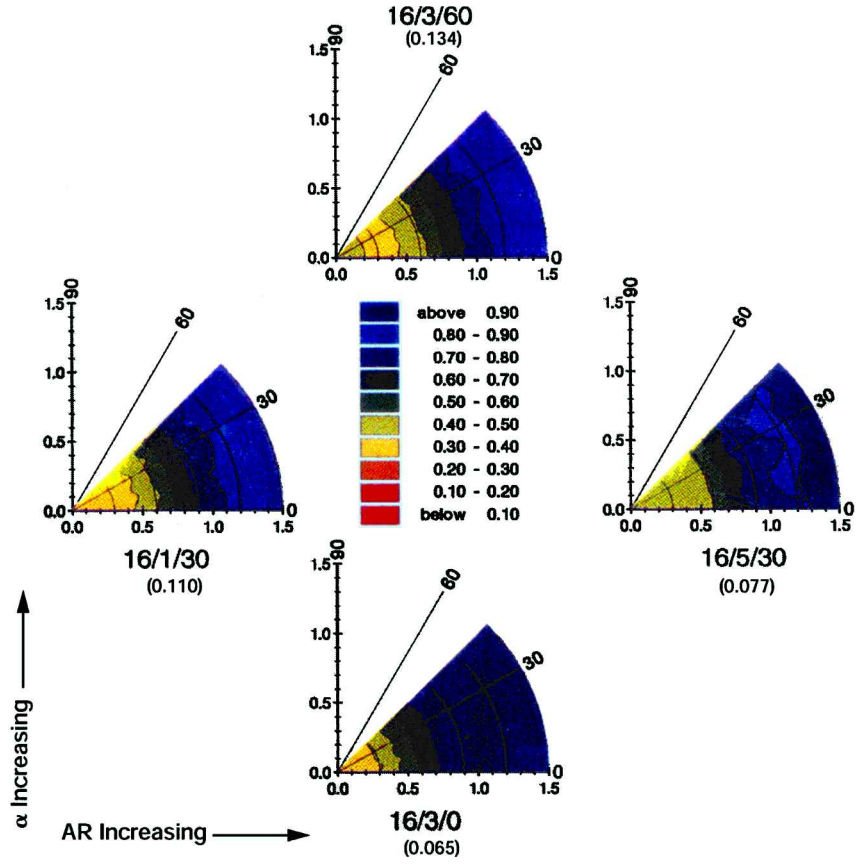

Fig. 5 Mixture fraction contours of 16 orifice modules at $z/r = 1.0$; numbers in parentheses are unmixedness values for each part of the figure.

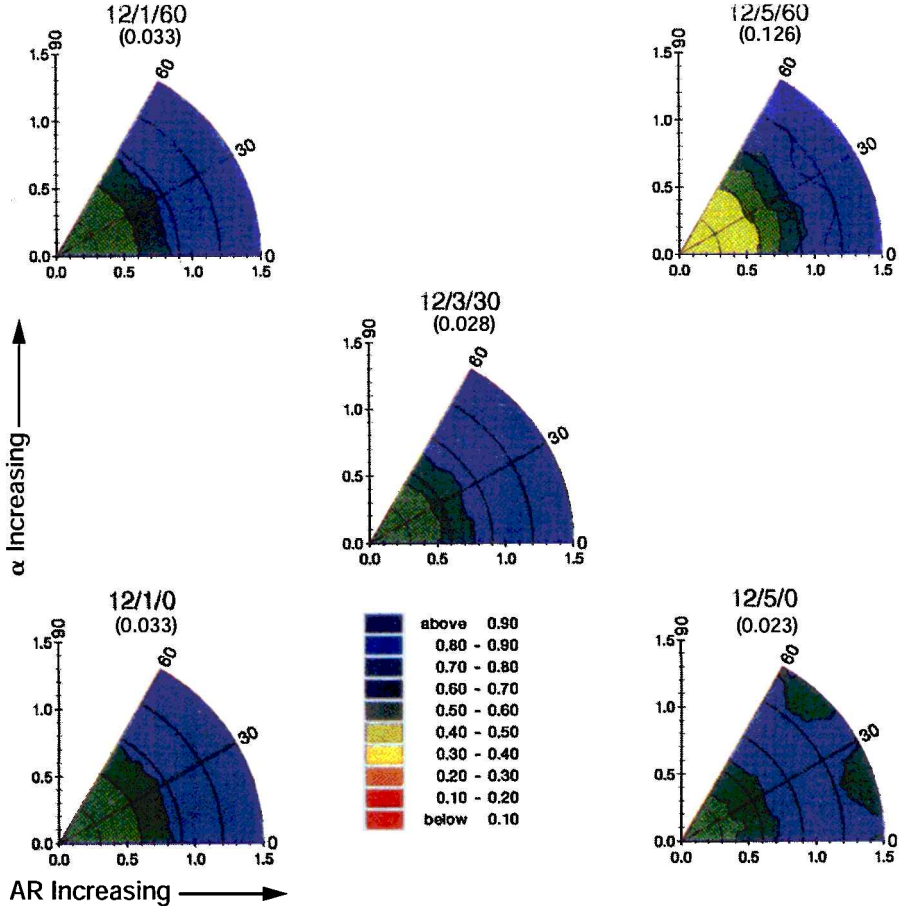

Fig. 6 Mixture fraction contours of 12 orifice modules at $z/r = 1.0$; numbers in parentheses are unmixedness values.

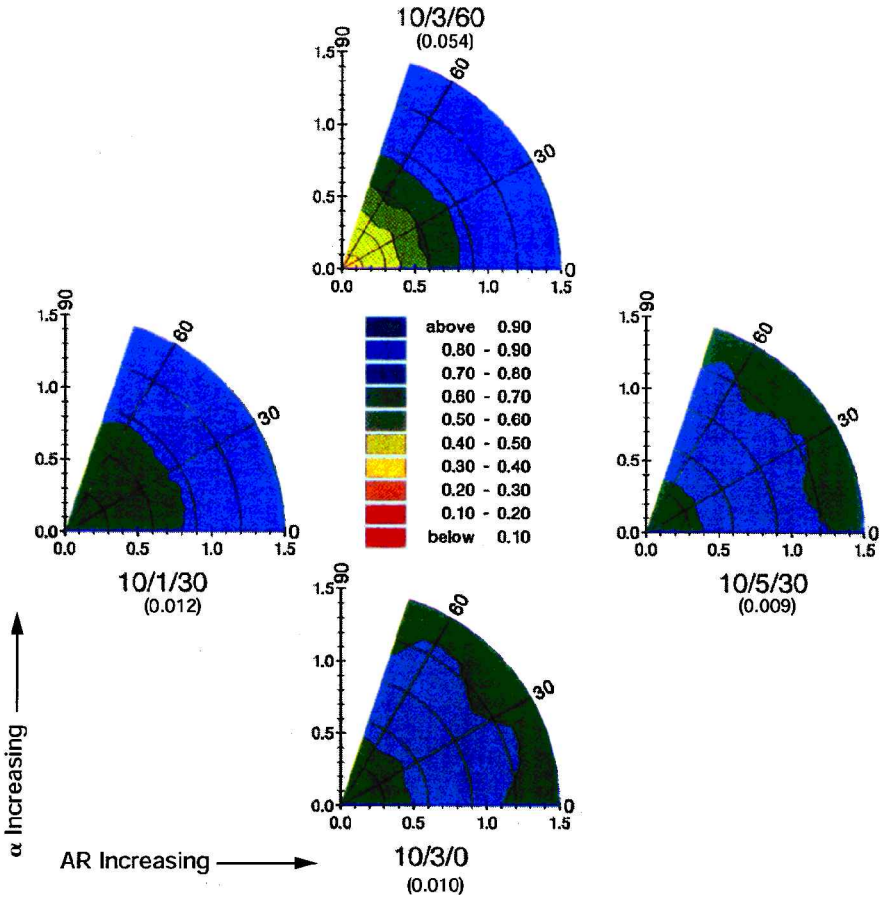

Fig. 7 Mixture fraction contours of 10 orifice modules at $z/r = 1.0$; numbers in parentheses are unmixedness values for each part of the figure.

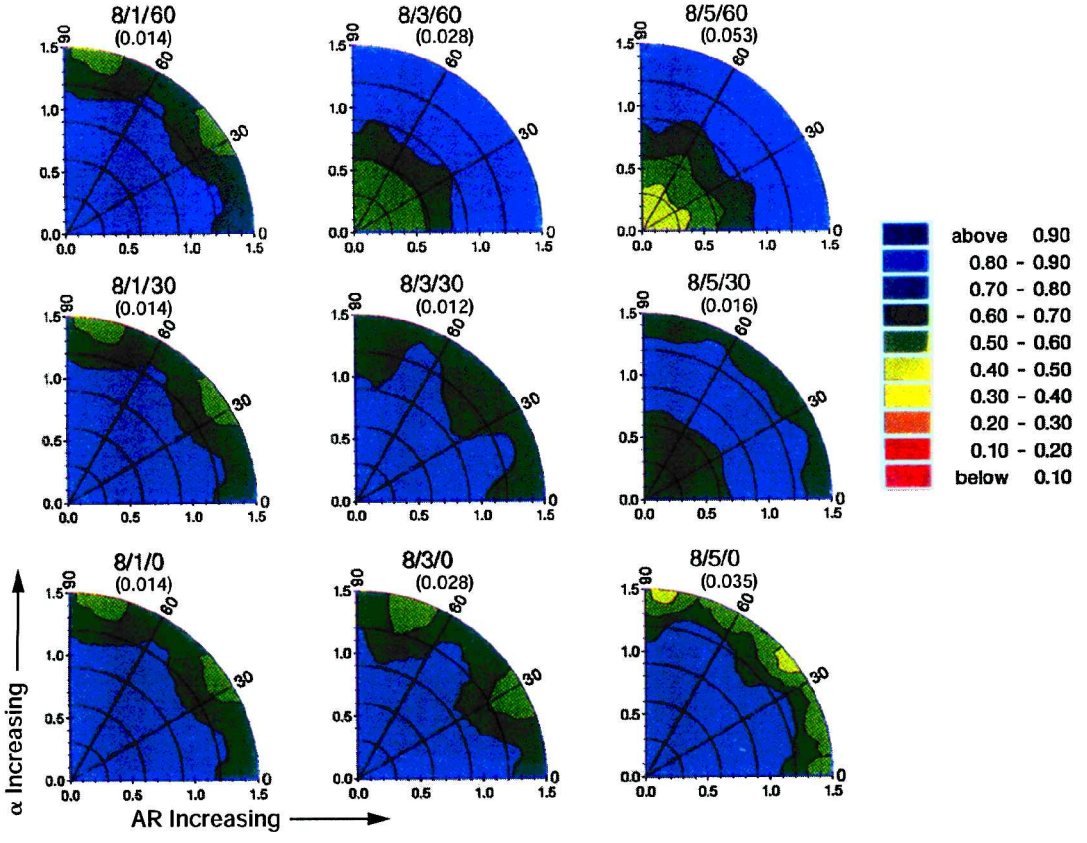

Fig. 8 Eight orifice modules' mixture fraction contours at $z/r = 1.0$; numbers in parentheses are unmixedness values for each part of the figure.

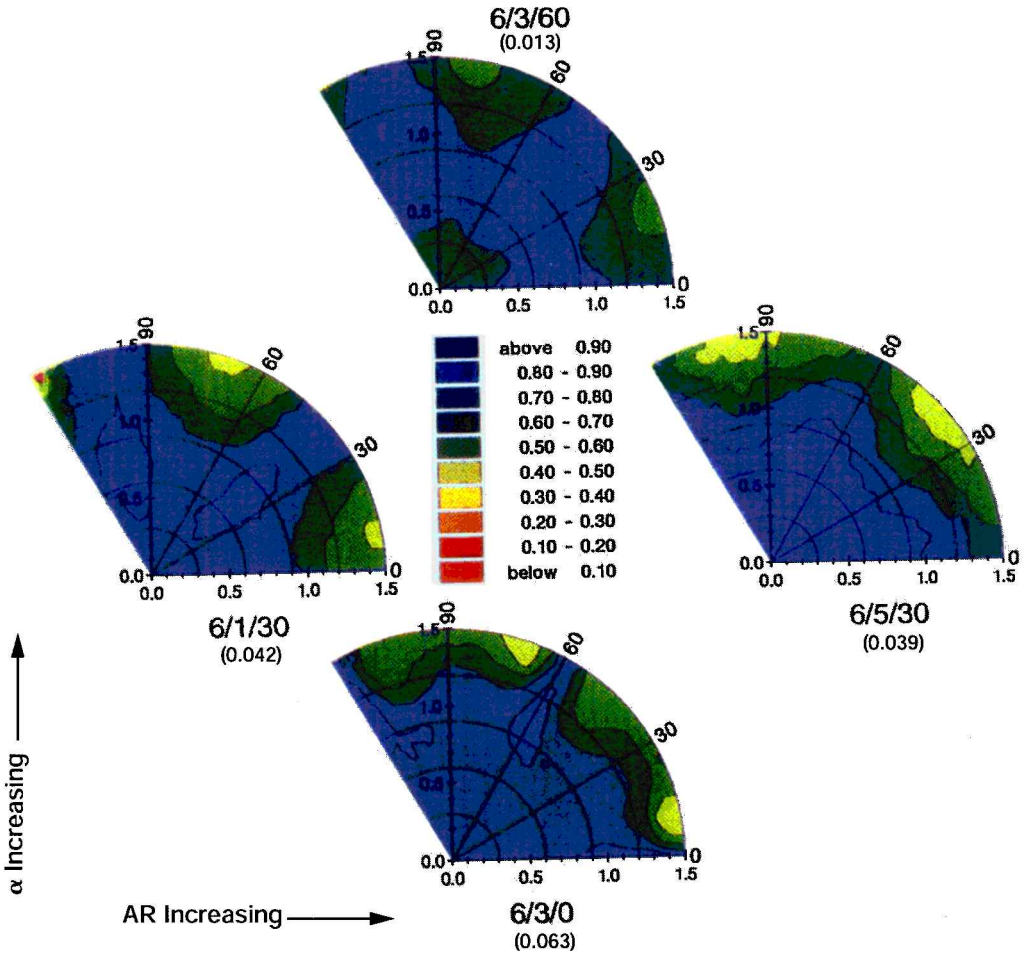

Fig. 9 Six orifice modules' mixture fraction contours at $z/r = 1.0$; numbers in parentheses are unmixedness values for each part of the figure.

angle could be uniquely specified at that condition. The numbers in parentheses are the unmixedness values [Eq. (3)] for the plane shown.

All 4 of the 16 orifice cases shown in Fig. 5 demonstrate underpenetrating jets. This is evident by the high mixture fraction values adjacent to the wall (blue) and low values on the mixer centerline (yellow). (If the jet penetration were balanced, a broad band of mixture fraction values containing the equilibrium value of 0.715 would be present with a band of slightly lower or higher mixture fraction values near the mixer centerline and wall.) For the 16-orifice case, the best value of unmixedness (closest to zero) is the 16/3/0 case, which is a slot aligned with the main flow. This is due to its having no induced swirl motion as do cases 16/3/60 and 16/5/30, and its having much less blockage than the 16/1/30 case.

As was seen with 16 orifices, the 12-orifice cases are largely underpenetrating (see Fig. 6). However, the mixing is, in some cases, much improved over the 16-orifice cases. The 12/5/0 case is the most balanced case and has the lowest spatial unmixedness for the 12-orifice cases. This, as was true for 16/3/0, results from a low blockage and no induced swirl because it is aligned with the main flow. The good mixing performance at one duct radius downstream is especially interesting given that the orifice axial length extends close to the evaluation plane.

Of all of the cases considered, the 10-orifice modules displayed the best mixing performance. In Fig. 7, only the 10/3/60 case displays significant underpenetration. This underpenetration is highly correlated with the swirl induced by the steep orifice angle. The sensitivity of mixing performance to blockage appears to be less important as the number of orifices approaches the optimum number. In the better-mixed cases, only two color ranges are represented that are close to the equilibrium mixture fraction value (0.715). As was discussed by Kroll et al.,[6] it can be seen that the optimum mean jet penetration depth falls between the half-area radius and the half radius as determined by the radial location where the lowest mixture fraction is measured in the evaluation plane.

The eight-orifice cases were the overlap condition between the two Box–Behnken test matrices discussed earlier. Therefore, more data planes are present than would be expected for either matrix alone. The seven cases are shown in Fig. 8. (Recall that the $AR = 1$ case is a round hole and is angle independent.) In the eight-orifice cases, jet underpenetration, balanced, and overpenetration are evident. The steep orifice angles still exhibit underpenetration likely due to the strong induced swirl. The no swirl cases, 8/5/0 and 8/3/0, show a tendency toward overpenetration. For eight orifices, however, the greater blockage of the 8/1/angle-independent case improves the mixing. The 8/5/30, 8/3/30, and 8/1/angle-independent cases all showed excellent mixing performance that is equivalent to the ten-orifice, good-mixing cases especially when considering the degree of case-to-case repeatability.

With six orifices (Fig. 9), only the steep-angled slanted slot orifice case 6/3/60 shows balanced jet penetration. The spatial unmixedness for this case is close to the best values measured in the 8- and 10-orifice cases. All of the other six-orifice cases are overpenetrating and consequently display degraded mixing performance. In some cases the orifice heights extend up to (6/3/0) and beyond (6/5/30) the evaluation plane.

Four repeat measurements were made for the eight round hole orifice case. The repeat cases were representative of the repeatability seen in all of the experiments. In general, the measured repeatability in the unmixedness was on the order of 0.008. The cases that had the steepest gradients in the measured mixture fraction generally had the worst repeatability.

Linear Regression Analysis

To further generalize the results, a linear regression was performed on 63 values of area weighted variance generated from the 26 cases noted using the Rummage II (see Ref. 13) statistical analysis software. An interpolating equation was created as a function of the three experimental parameters (n = number of orifices, AR = orifice aspect ratio, and α = orifice slant angle). Insignificant terms were eliminated from the model using conventional statistical methods. The regression model took into account that at an AR of 1, the result had to be angle independent. The regression data were scaled to remove any unnecessary ill conditioning due to the data ranges considered. The resulting equation is

$$\sqrt{U_S} = \left(C_0 + C_1 * \chi_1 + C_2 * \chi_2 + C_3 * \chi_3 + C_4 * \chi_1^2 + C_5 * \chi_3^2 + C_6 * \chi_1 * \chi_2 + C_7 * \chi_1 * \chi_3 + C_8 * \chi_2 * \chi_3 + C_9 * \chi_1^3 + C_{10} * \chi_1^2 * \chi_3\right) \Big/ \sqrt{\bar{f}(1-\bar{f})} \tag{4}$$

where

$$\chi_1 = \frac{n - 10.286}{3.367}, \qquad \chi_2 = \frac{AR - 2.239}{1.583}$$

$$\chi_3 = \frac{[\alpha * (AR - 1)] - 37.143}{65.928}, \qquad \bar{f} = 0.715$$

$$C_0 = 0.0594, \quad C_1 = 0.0266, \quad C_2 = -0.0045$$

$$C_3 = 0.0119, \quad C_4 = 0.0276, \quad C_5 = 0.0102$$

$$C_6 = -0.0139, \quad C_7 = 0.0183, \quad C_8 = -0.0091$$

$$C_9 = -0.0091, \quad C_{10} = -0.0081$$

The regression equation had a correlation coefficient of 0.926 and an estimated standard deviation of 0.011. Although potential outliers were identified in the data set, no data were removed when fitting the regression equation. Not removing the outliers resulted in 6 of the 63 data points accounting for 46.6% of the regression sum of squares error.

Figure 10 shows the predicted values of U_S as number of orifices, orifice AR, and orifice angle are changed. Many of the observations made in the preceding figures (Figs. 5–9) can be more easily seen. First, only in the six-orifice case is the steep-angled slot at a high AR an advantage. As the number of orifices increases, the performance of the steep-angled slot at a high AR becomes more and more degraded. At a high number of orifices, a zero-angled slot with a high aspect is the best. Second, the highly nonlinear relationship between the three controlled variables is evident. It was this highly nonlinear relationship that required introducing third-order cross terms into the correlation equation. Third, it appears that the optimum number of orifices falls between eight and ten when the unmixedness is the optimizing parameter. Fourth, it is also evident that in the near-optimum configuration, the orifice AR is of lesser importance as long as the orifice angle is shallow. However, as emphasized in Refs. 1–3, a single parameter, such as U_S, can help identify an optimum mixer, but must be examined in the context of the distributions.

The independence of orifice AR when using shallow-angled orifices at the optimum number of orifices is better understood by considering a contour plot for the nine-orifice case shown in Fig. 11. In Fig. 11, two optimums are present. One optimum is at an AR of 1 and the second optimum is at an AR of 5 and an orifice angle of 20. Given the uncertainty in the measurements (discussed earlier), one would expect equally good mixing performance at many combinations of shallow-angled slanted slots and ARs. The existence of two optimums is also predicted in the 8- and 10-orifice cases. When the orifice number increases beyond 10, only one optimum is predicted at high ARs and shallow angles.

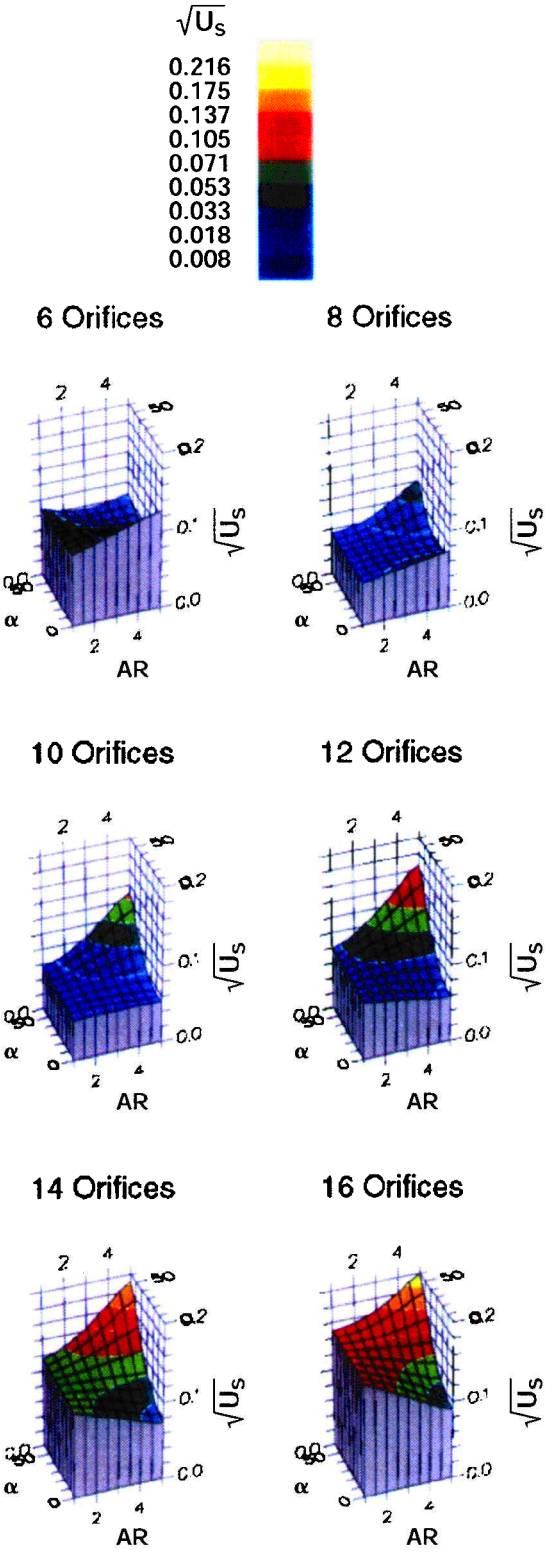

Fig. 10 Predicted values of spatial unmixedness for different orifice numbers as orifice aspect ratio and orifice angle are changed.

In an effort to verify the existence of two optimums, two additional cases were considered: 9/1/angle-independent and 9/5/22. The contour plots for these cases are shown in Fig. 12. The 9/1/angle-independent case demonstrated an experimentally derived spatial unmixedness of 0.013, which is close to the predicted value. The 9/5/22 case displayed greater jet penetration to the centerline than expected. This resulted in an experimentally derived unmixed-ness of 0.021, which is higher than the predicted value of 0.013. Because

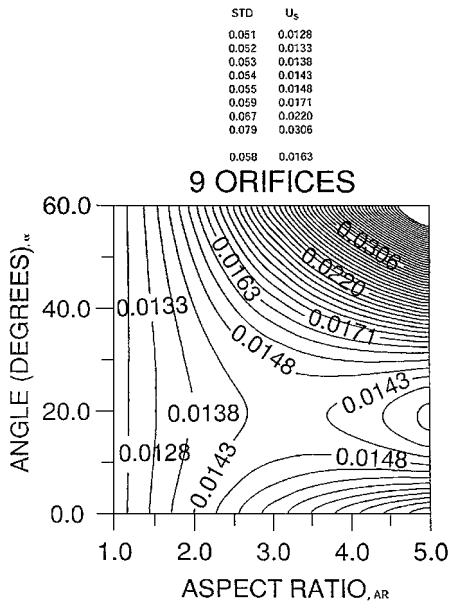

Fig. 11 Predicted values of spatial unmixedness U_S for the nine orifice case as orifice AR and orifice angle are changed.

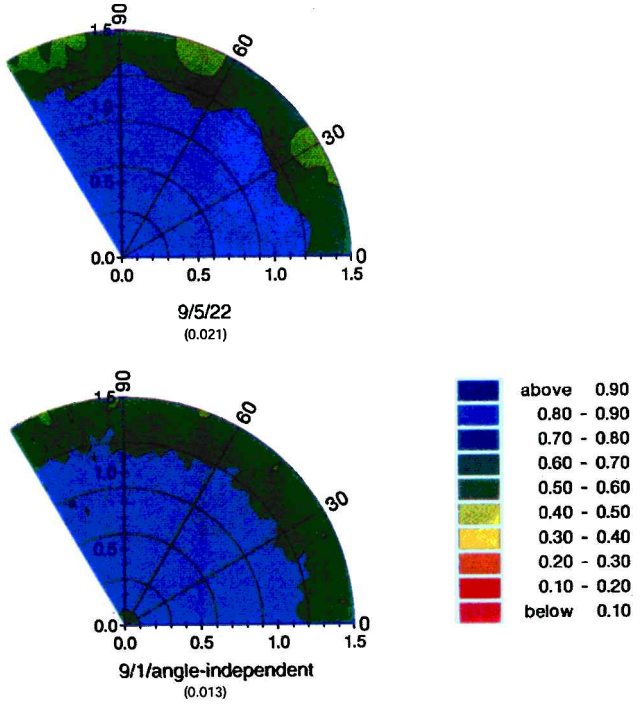

Fig. 12 Nine orifice modules' mixture fraction contours at z/r = 1.0; numbers in parentheses are unmixedness values.

the repeatability of the measurement of U_S (as discussed earlier) is on the order of 0.008, the 9/5/22 result is within the uncertainty band. However, this experimental result for the 9/5/22 case is somewhat anomalous because the 10/5/30 and the 8/5/30 cases (see Figs. 7 and 8) both display balanced jet penetration. It is, however, possible that the nonlinear sensitivity of the interpolating equation is not sufficient. Consider, for example, that the 8/5/0 case does display jet overpenetration.

Conclusions

This study focused on the relationship between number of orifices, orifice AR, and orifice angle at a fixed momentum-flux ratio (40) in a plenum fed cylindrical can mixer. The mixture fraction field at one duct radius downstream of the leading edge of the orifices was measured experimentally using thermocouples in a nonreacting flowfield. The mixture fraction fields as well as the spatial unmixedness values were used to assess mixing performance. A general interpolating equation was found using least-squares regression that was used to further elucidate the trends. The optimization experiments resulted in the following conclusions:

1) Mixture uniformity is a nonlinear function of the number of orifices, the orifice long-to-short AR, and the orifice angle.

2) Jet penetration depth is a function of circumferential blockage, orifice spacing axial jet mass addition rate, and orifice-induced swirl.

3) Optimum mixing occurs when the asymptotic mean jet trajectories at $x/R = 1.0$ are in the range of $0.30 < \zeta/R < 0.5$ (where $\zeta = R - r$).

4) An optimum number of orifices exists for a given momentum-flux ratio that minimizes the unmixedness value. Although an overall minimum for a given momentum-flux ratio can be established, a local minimum for a given number of orifices occurs as well. Thus, the appropriate configuration may depend on given values of both the momentum-flux ratio and the number of orifices.

5) When the optimum number of orifices is exceeded, underpenetration is expected, and steep-angled slanted slots lead to extremely poor mixing performance, punctuated by degraded penetration. In this case, aligned slots that minimize the blockage without inducing swirl provide the best mixing performance.

6) At the optimum number of orifices, the difference between shallow-angled slots with large ARs and round holes is minimal and either approach yields good mixing performance. At the optimum number of orifices, two local optimums can exist where one corresponds to a round hole and the second to a shallow-angled slanted slot.

7) When the number of orifices is below the optimum number, overpenetration is expected with an advantage to having steep-angled slanted slots at a high AR. In this case, the slot-induced swirl minimizes the degree of overpenetration.

8) Understanding how the number of slots, orifice AR, and orifice angle relate to one another provides a means to further address design issues as load changes in devices that rely on jet mixing as an inherent part of their operation.

Acknowledgment

This work was made possible by support provided by NASA John H. Glenn Research Center at Lewis Field (Grant NAG3-1110).

References

[1]Holdeman, J. D., Liscinsky, D. S., Oechsle, V. L., Samuelsen, G. S., and Smith, C. E., "Mixing of Multiple Jets with a Confined Subsonic Crossflow: Part I—Cylindrical Ducts," *Journal of Engineering for Gas Turbines and Power*, Vol. 119, No. 4, Oct. 1997, pp. 852–862; also American Society of Mechanical Engineers, Paper 96-GT-482, June 1996 and NASA TM-107185.

[2]Holdeman, J. D., Liscinsky, D. S., and Bain, D. B., "Mixing of Multiple Jets with a Confined Crossflow: Part II—Opposed Rows of Orifices in Rectangular Ducts," *Journal of Engineering for Gas Turbines and Power*, Vol. 121, No. 3, July 1999, pp. 551–562; also American Society of Mechanical Engineers, Paper 97-GT-439, June 1997, and NASA TM-107461.

[3]Holdeman, J. D., "Mixing of Multiple Jets with a Subsonic Crossflow," *Progress in Energy and Combustion Science*, Vol. 19, 1993, pp. 31–70; also NASA TM-104412.

[4]Margason, R. J., "Fifty Years of Jet in Cross Flow Research," Computational and Experimental Assessment of Jets in Cross Flow Meeting, AGARD April 1993.

[5]Hatch, M. S., Sowa, W. A., Samuelsen, G. S., and Holdeman, J. D., "Jet Mixing into a Heated Crossflow in a Cylindrical Duct: Influence of Geometry and Flow Variations," *Journal of Propulsion and Power*, Vol. 11, No. 3, 1995, pp. 393–402; also NASA TM-105390.

[6]Kroll, J. T., Sowa, W. A., Samuelsen, G. S., and Holdeman, J. D., "Optimization of Circular Orifice Jets Mixing Into a Heated Crossflow in a Cylindrical Duct," AIAA Paper 93-0249, Jan. 1993; also NASA TM-105984.

[7]Oechsle, V. L., Mongia, H. C., and Holdeman, J. D., "Analytical Study of Jet Mixing in a Cylindrical Duct," AIAA Paper 93-2043, June 1993; also NASA TM-106181.

[8]Hatch, M. S., Sowa, W. A., and Samuelsen, G. S., "Influence of Geometry and Flow Variation on Jet Mixing and NO Formation in a Model Staged Combustor Mixer with Eight Orifices," Univ. of California, Irvine; also NASA CR-194473, June 1996.

[9]Kroll, J. T., Sowa, W. A., and Samuelsen. G. S., "Optimization of Orifice Geometry for Cross-Flow Mixing in a Cylindrical Duct," Univ. of California, Irvine; also NASA CR-198482, April 1996.

[10]Smoot, L. D., and Smith, P. J., *Coal Combustion and Gasification*, Plenum, New York, 1985.

[11]Liscinsky, D. S., True, B., and Holdeman, J. D., "Experimental Investigation of Crossflow Jet Mixing in a Rectangular Duct," AIAA Paper 93-2037, July 1993; also NASA TM-106152.

[12]Danckwertz, P. V., "The Definition and Measurement of Some Characteristics of Mixtures," *Applied Scientific Research*, Sec. A, Vol. 3, 1952, pp. 279–296.

[13]Bryce, G. R., "Data Analysis in RUMMAGE—A User's Guide," Dept. of Statistics, Brigham Young Univ., Provo, Utah, Nov. 1982.

Color reproductions courtesy of NASA John H. Glenn Research Center at Lewis Field.